Chemical Engineering Journal 486 (2024) 150355

Contents lists available at ScienceDirect

Chemical Engineering Journal

journal homepage: www.elsevier.com/locate/cej

Deformation and rupture of Janus nanoparticle-stabilized Pickering emulsion in confined channel

Yuanhao Chang [a,b], Senbo Xiao [a,*], Rui Ma [a], Zhiliang Zhang [a], Fanhua Zeng [b,*], Jianying He [a,*]

[a] Department of Structural Engineering, Norwegian University of Science and Technology (NTNU), 7491 Trondheim, Norway
[b] Petroleum Systems Engineering, Faculty of Engineering and Applied Science, University of Regina, Regina, Saskatchewan S4S 0A2, Canada

ARTICLE INFO

Keywords:
Pickering emulsion
Janus nanoparticle
Surface coverage
Nanomechanical property
Molecular dynamics simulation

ABSTRACT

The interaction between Pickering emulsions and confined channels is vital for their industrial applications. However, how solid particle shells modulate the deformation stability and rupture limit of Pickering emulsions in contact with wall remains poorly understood. In this work, mechanical deformation and rupture of Janus nanoparticles (JNP)-stabilized Pickering emulsions on solid surfaces are elaborated by molecular dynamics (MD) simulations. A universal master-type predictive model is developed for the first time to describe the contact behavior of Pickering emulsions against surfaces with distinct wettability. The contact stress of an emulsion is determined by the equivalent elastic modulus of the emulsion, geometric deformation function, and the influence of the JNP shell and its interactions. Moreover, hydrophobic surfaces lead to the rupture of Pickering emulsions in compression. The rupture can be delayed by increasing JNP surface coverage (ϕ). Especially, once ϕ reaches a critical value, the JNP shell can form an ordered quasi-solid structure, significantly enhancing the emulsion stability. These results can aid in the design or screening of specific Pickering emulsions to manage their deformation and rupture on the solid surface, in applications ranging from water treatment and drug delivery to environmental remediation and mobility control in oil recovery.

1. Introduction

Pickering emulsions, which were introduced around 100 years ago, are emulsions stabilized by solid particles instead of organic surfactants and polymers [1,2]. Adsorbed solid particles form a steric hindrance to prevent the coalescence between droplets [3–5]. Compared to conventional emulsions, Pickering emulsions have superior stability and high internal payload capacity and are considered to be less toxic [6,7]. Therefore, they not only provide a unique platform for synthesizing colloidal nanocomposites and interfacial catalysis for product separation [8–11], but also exhibit great application potential in various industrial sectors such as water treatment [12], interfacial catalysis [13], food technology [14], environmental remediation [15], oil recovery [16] and drug delivery [17].

The stability of emulsion droplets holds significant importance in various applications [18]. However, there are cases where destabilization of these droplets becomes necessary. For example, in topical medications, emulsion droplets need to maintain stability during storage but require destabilization for localized delivery of the active ingredient [19]. Consequently, extensive global attention has been drawn to the investigation of Pickering emulsion stability [20,21]. At present, there has been substantial research conducted on the stabilization and destabilization mechanisms of Pickering emulsion systems, specifically the interactions between emulsion droplets [22,23]. Although numerous factors influencing stability have been identified [22–25], the relationship between surface coverage and emulsion stability remains ambiguous under current characterization methods [23]. Considering that the solid particles responsible for stabilizing Pickering emulsions define their unique properties, the role of surface coverage becomes important in determining emulsion stability. Hence, it is imperative to place greater focus and employ improved characterization techniques to examine the impact of surface coverage on emulsion stability.

To ensure the stability of Pickering emulsion in confined channels, understanding their mechanical properties is crucial [19]. The situations encompass not only the extrusion and friction experienced by emulsions in the oral cavity or gastrointestinal tract during drug delivery [26], but also the adsorption and retention of Pickering emulsions in porous media of oil reservoirs during enhanced oil recovery [27]. Assessing the stability of emulsions in these cases involves examining the mechanical deformation or rupture of the droplet under compression against solid

* Corresponding authors.
E-mail addresses: senbo.xiao@ntnu.no (S. Xiao), fanhua.zeng@uregina.ca (F. Zeng), jianying.he@ntnu.no (J. He).

https://doi.org/10.1016/j.cej.2024.150355
Received 12 December 2023; Received in revised form 21 February 2024; Accepted 10 March 2024
Available online 11 March 2024

surfaces [28]. Despite limited research on this topic, atomic force microscopy (AFM) is an adopted research technique that can measure the elasticity of individual emulsion droplets. Furthermore, the droplet shape can be monitored using reflection interference contrast microscopy (RICM) or laser scanning confocal microscopy (LSCM). A combination of these approaches has successfully revealed the nanomechanical properties of single emulsion droplets stabilized by spherical biological nanoparticles [29]. However, accurately probing the structural changes of solid particle shells (surface coverage and distribution of solid particles) and characterizing the interfacial interactions of Pickering emulsion remains challenging. Thus, the role of the solid particle shell in the deformation and rupture of emulsions remains elusive.

Molecular dynamics (MD) simulation shows great potential in gaining microscopic insights into the stability mechanism of Pickering emulsion, including the mechanical properties of the emulsion, the structure and interfacial behavior of solid particle stabilizers, and their interactions with multiphase fluids and surfaces [30,31]. MD simulations have been applied to reveal the nanoscale behaviors of particles in ultra-small channels [37,38], the oil–water emulsification and demulsification processes [39,40], and the nanomechanical properties of a given emulsion system [41]. Moreover, dissipative particle dynamics (DPD) simulations were carried out by Fan and Striolo to investigate the coalescence process of nanoparticle-stabilized Pickering emulsions [32]. The work confirmed the excellence of Janus nanoparticles (JNPs) in stabilizing Pickering emulsions and the important phenomena involved in the stabilization mechanism. Nevertheless, to the best of our knowledge, there are currently no molecular or atomic simulations on the mechanical deformation and rupture characteristics of the individual Pickering emulsion.

In this study, the targeted Pickering emulsion is stabilized by JNPs whose surface has two distinct parts with varied wettability [33]. First of all, Pickering emulsions with specific JNP surface coverage (ϕ) are selected through the equilibration stage in the MD simulations. Subsequently, the characteristics of deformation and rupture of emulsions on solid hydrophilic or hydrophobic surfaces are assessed with nanoscale compression tests. A generic model that can describe the universal behavior of Pickering emulsion in contact with solid surfaces is for the first time developed. Finally, the factors that govern the rupture of Pickering emulsions on the surface are unraveled by careful analysis of the structural change of JNP shells. The findings provide insights into the deformation and rupture of Pickering emulsion on solid surfaces and facilitate the design and preparations for Pickering emulsion in industrial applications.

2. Model and simulation details

2.1. Model

The focus of the study is Pickering emulsion stabilized by JNPs, as depicted in Fig. 1(a). The oil droplet is assembled by hexane molecules using the Packmol codes [34]. Spherical JNPs with a diameter of 10 Å are uniformly distributed on the surface of the oil droplets as the JNP shell. All non-polar atoms are oriented toward the oil core. In the reference group, the oil core is 70 Å in diameter and contains 920 hexane molecules. The number of JNPs increases from 30 to 100, corresponding to a change in surface coverage from 0.28 to 0.91. The molecular system representing the nanomechanical test of Pickering emulsion on the surface is shown in Fig. 1(b). The system has a volume of 131 × 190 × 200 $Å^3$ with a periodic boundary condition. The silicon substrate is placed on the left of the system, with a thickness of 12 Å. The wettability of the surface is modified in the study, to explore the varied stability of the emulsion. The Pickering emulsion is placed in the middle of the system. Water molecules fill the rest of the box with a density of 1003 kg/m^3.

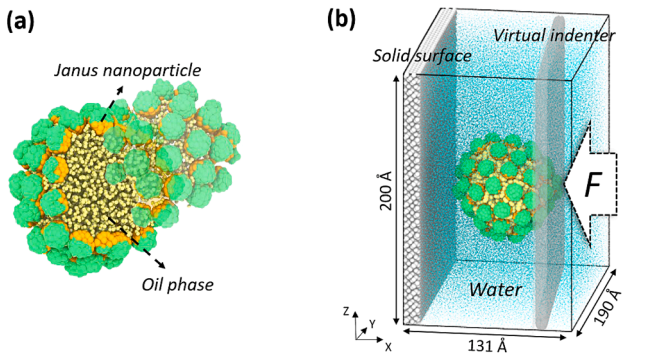

Fig.1. The schematic of the model: (a) the Pickering emulsion, (b) and the initial structure of the simulation system. The white arrow shows the force direction. The colors for different components: water (light blue), oil (yellow), solid surface (grey), hydrophobic beads (orange), and the hydrophilic beads of JNP (green).

2.2. Force field

The mW water model is adopted for the water molecules, while the Transferable Potentials for Phase Equilibria united-atom (TraPPE-UA) description of hexane is employed for the oil core [35,36]. To be specific, the Stillinger–Weber (SW) potential is for the water-water non-bonded interactions, while the standard pairwise 12–6 Lennard-Jones (LJ) potential is for water–oil and oil-oil non-bonded interactions [37]. The atomistic interaction parameters pertaining to the surface and JNPs are derived from our previous studies [38,39]. The specific values of characteristic energy are presented in Table S1, and the wettability test of hydrophilic and hydrophobic surface are provided in Fig. S1. All the atoms in the systems are free of charge.

2.3. Simulation strategy and process

All the MD simulations are performed with the LAMMPS package [40] and visualized with OVITO software [41]. The systems are first energy-minimized using the steepest descent method and followed by a 50 ns equilibrium stage in the NVT ensemble at a temperature of 350 K. The Nosé–Hoover thermostat with a coupling coefficient of 100 fs is adopted in the simulations [42,43]. Afterward, a virtual plane indenter is set on the right of the emulsion (Fig. 1(b)). The indenter moves toward the emulsion with a constant speed of 10^{-5} Å/fs. In order to improve simulation efficiency and also to avoid the excessive loading rate of the force, the force constant of the indenter is kept as 10^{-3} kcal/mole $Å^{-3}$. In the simulation, the force applied on the emulsion is obtained by recording the counterforce on the indenter every 2000 fs. Besides, to accelerate the simulation, JNPs are treated as the rigid body, and the solid surface is positionally fixed. Five independent simulations are employed in each case for the significance of the results.

3. Results and discussion

3.1. Equilibration and selection of the Pickering emulsion

To ensure the stable status of the sphere-like Pickering emulsion in the subsequent nanomechanical test, 50 ns equilibration for Pickering emulsions with different surface coverage (ϕ) is employed. It is worth noting that when the surface of the oil core is covered with a large number of JNPs, local JNPs tend to aggregate into clusters [44]. As a result, an unbalanced force is generated on the droplet, leading to the overall deformation of the emulsion. Therefore, the optional range of ϕ should also be determined in the equilibration of the Pickering emulsion, in addition to providing the stable configuration. Referring to the previous MD study of spherical JNPs at the oil–water interface, the

initial range of ϕ is chosen from 0.28 to 0.91 [44].

In order to quantify the shape of the droplet in each case, the asphericity (κ) of the emulsions after the equilibrations are calculated (Fig. 2) [45]:

$$\kappa^2 = \frac{3}{2}\frac{\alpha_1^4 + \alpha_2^4 + \alpha_3^4}{\left(\alpha_1^4 + \alpha_2^4 + \alpha_3^4\right)^2} - \frac{1}{2} \quad (1)$$

where α_1, α_2, and α_3 are the coordinates along the three directions of the coordinate axis. By definition, as the emulsion is closer to the sphere, the value of asphericity tends to be 0. Obviously, the asphericity of the emulsion with ϕ of 0.82 and 0.91 is high, with the shape becomes nonspherical (as shown in Fig. 2). Besides, it should be mentioned that when ϕ is small (at 0.28), the value of asphericity is also relatively large. This may originate from the uneven distribution of JNPs on the surface. In this work, the droplet with asphericity below 0.05 is regarded as the spherical one. Thus, the Pickering emulsions with ϕ ranging from 0.28 to 0.73 are selected for the nanomechanical properties research.

3.2. Compression dynamics and mechanical response

The nanoscale compression of an emulsion on solid surfaces with varied wettability is simulated. The behavior of deformation or potential rupture in the Pickering emulsion, along with the observed mechanical response, characterizes its inherent resistance to deformation and nanomechanical properties.

3.2.1. Compression of Pickering emulsion on a hydrophilic surface

For the case with a hydrophilic surface, the representative compression process (emulsion with ϕ of 0.46) is shown in Fig. 3(a): the emulsion deforms continuously but a final rupture does not occur. As compression force is removed, the emulsion quickly recovers its original shape, indicating the deformation is elastic. For comparison, two important mechanical quantities, the nominal strain which is defined as the length change divided by the original length of the Pickering emulsion along the direction of the applied force, and the nominal stress which is defined as the applied load divided by the original maximum cross-sectional area of the emulsion, are calculated. The nominal stress–strain curves of the emulsions with various ϕ are recorded in Fig. 3(b). The stress–strain curves exhibit the obvious differences as the strain is over ca. 30 %. Specifically, when ϕ is below 0.55, the stress increases with increasing ϕ under the same strain. While once ϕ reaches 0.55, the stress values among different emulsions exhibit little variation. For the stress in all the cases, it increases gradually when the strain is below ca. 20 %, and then significantly elevates at high strain value. The results from the atomistic simulations are consistent with the experiment [19]. The normalized strain energy of each emulsion, representing its deformation capacity, is calculated by integrating the respective strain-strain curve shown in Fig. 3(b) up to a strain of 60 %. The comparison of these normalized strain energies is presented in Fig. 3(c). It can be observed from Fig. 3(c) that, although the difference is minor, the strain energy of the emulsion progressively increases and remains the high level after ϕ reaches 0.55. The observation reveals that extra JNPs enhance the emulsion's resistance to deformation at low ϕ values while such effect diminishes once ϕ surpasses 0.55. Generally, the overlapping of the stress–strain curves and small variation of the strain energy indicate there is a similarity regarding the compression behavior of Pickering emulsion against a hydrophilic surface among the emulsions with various degrees of surface coverages. The stress–strain curve obtained from any emulsion can be regarded as the "universal or master mechanical behavior" of the whole family of emulsions under compression against hydrophilic surfaces. The insensitivity of compression response to the surface coverage attributes to the weak attraction force by solid surface and the preservation of mechanical integrity of the emulsion during the whole compression process.

3.2.2. Compression of Pickering emulsion on a hydrophobic surface

In the case of a hydrophobic surface, the Pickering emulsion is highly likely to rupture due to the strong interactions between the oil core and the surface. The representative deformation snapshots are shown in Fig. 4(a). During the compression, the oil core of the emulsion is constantly approaching the surface. Once oil molecules make contact with the surface (the third snapshot in Fig. 4(a)), the emulsion ruptures rapidly (the fourth snapshot in Fig. 4(a)). The variation of force, strain, and oil core-water interactions during the compression are collected in Fig. S2, with three stages marked (emulsion moving, deformation, and rupture). Initially, the emulsion is pushed toward the solid surface by the applied force. While the force gradually increases, the strain of the emulsion droplet remains at approximately zero. Upon contact with the solid surface, the emulsion starts to deform, eventually leading to its rupture. After the rupture of the emulsion, the interaction between the oil core and water exhibits an interesting hill-shaped variation (Fig. S2 (c)). In combination with the snapshots in Fig. S3, it can be observed that the oil core is first covered by the JNP shell on the surface after the rupture. The interaction between the oil core and water is thus partially shielded by the surface and JNP shell. However, due to the attraction force exerted by the hydrophobic surface, the oil core further collapses and spreads along the surface, significantly enhancing the interaction

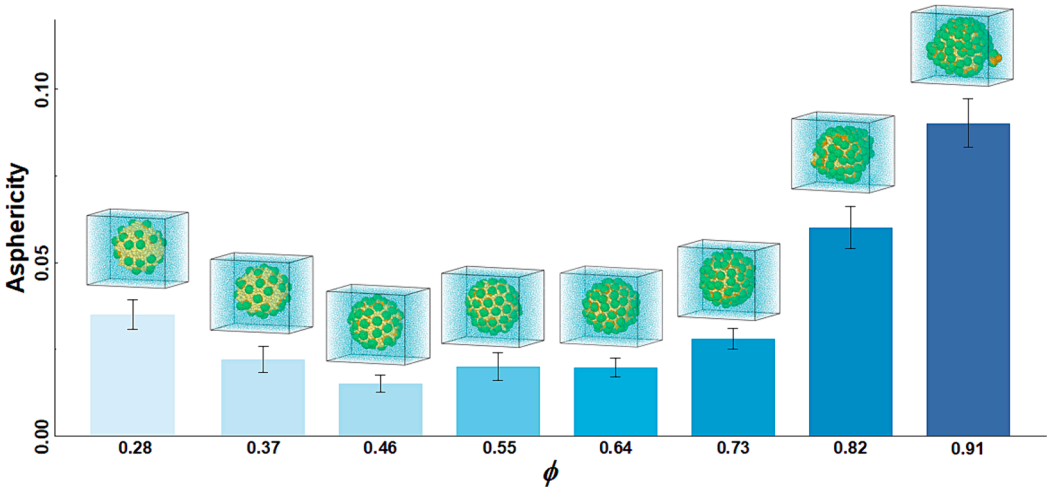

Fig.2. Asphericity for emulsions with varied ϕ. The error bar indicates the standard deviation of 5 independent simulations. The snapshots of varied ϕ after equilibration.

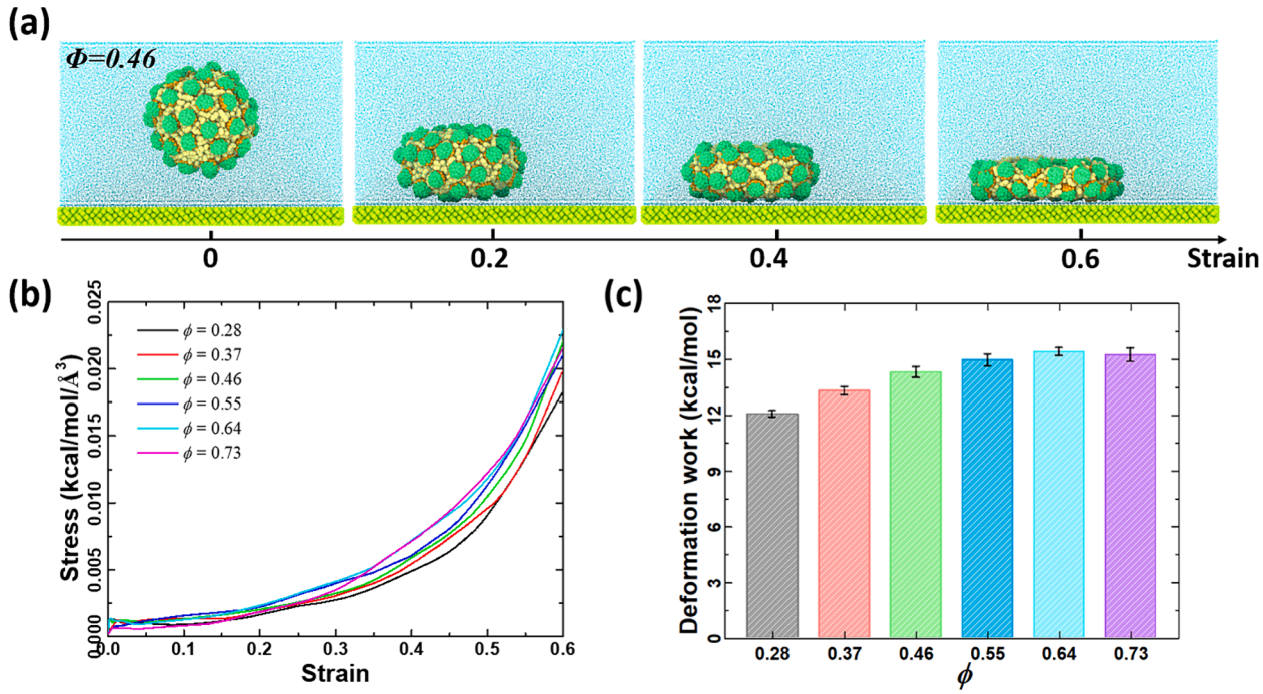

Fig.3. The compression of Pickering emulsion on the hydrophilic surface. (a) The representative snapshots in the compression. (b) The nominal stress–strain profiles for emulsions with different ϕ. (c) The deformation work for emulsions with different ϕ.

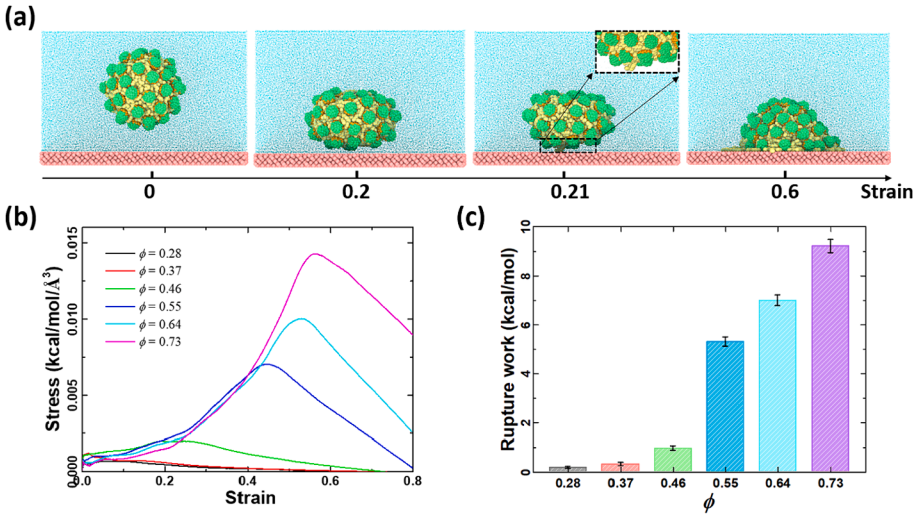

Fig.4. Compression of Pickering emulsion on the hydrophobic surface. (a) The representative snapshots (emulsion with ϕ of 0.46) in the compression. (b) The stress–strain profiles in the compression of emulsions with different ϕ. (c) The rupture work for emulsions with different ϕ.

between oil and water.

The stress–strain profiles of emulsion with varying ϕ under compression are further presented in Fig. 4(b). The peaks in the graphs correspond to the rupture force observed at the rupture moment (as represented in the third snapshot in Fig. 4(a)). It can be observed that before rupture, all the emulsions approximately follow the same curve independent of the surface coverage. The surface coverage, however, strongly dictates the rupture, namely, the critical strain beyond which the rupture occurs. The larger ϕ is, the greater strain at rupture. This can be attributed to the presence of more JNPs around the oil core, which forms a denser protection shell that effectively impedes the interaction between the oil core and the surface, hence delaying the emulsion rupture. Besides, it is noteworthy that emulsions with ϕ less than 0.55 exhibit considerably lower rupture work (Fig. 4(c)), whereas those with larger ϕ show a marked increase in required rupture work. Accordingly, the mechanical stability of the Pickering emulsion with ϕ of 0.55 is drastically improved. This suggests the existence of a critical ϕ in controlling the stability of the emulsion structure, which will be further investigated in the following sections.

3.2.3. *Droplet size effect*

Droplet size has a remarkable influence on the stability, control release, and rheology of emulsions [46]. In order to investigate its effect on the mechanical property of emulsion, the same nanoscale compression test is performed on two additional groups of Pickering emulsions with droplet radii of 25 Å and 30 Å. Also, a ϕ range of 0.28 to 0.73 is designed for each group of emulsions. This means that emulsions with the same ϕ but different radii possess different numbers of JNPs.

The stress–strain profiles of emulsions, differentiated by droplet sizes, during compression on a hydrophilic surface, are depicted in Fig. S4. It's shown that greater stress is required for the smaller size emulsions at the same strain. That's to say, the emulsion with a smaller size exhibits greater stiffness, in agreement with the finding in microcapsule compression experiments [47]. Furthermore, the quantitative relationship of the ϕ and droplet size of the Pickering emulsions on elastic modulus can be determined by using Hertzian elastic contact model [48]. By fitting the nominal stress–strain curves in Fig. S4 within the strain range of 0–3 %, the reduced elastic modulus (E^*) are recorded in Fig. 5(a). Obviously, the Pickering emulsion with a small droplet size possesses a greater elastic modulus. In comparison, ϕ of emulsion has a limited effect on the modulus, with a potential peak at ϕ of 0.55.

Furthermore, the effect of droplet size on emulsion rupture is explored with the compression test on the hydrophobic surface. The stress and strain at rupture of emulsions are recorded in Fig. 5(b) and (c), respectively, based on the collected stress–strain profiles (Fig. S5). Generally, larger droplet sizes result in more stable emulsions that can withstand greater stress and allow for greater strain at rupture. However, it should be noted that the effect of droplet size is only apparent in emulsions with a large value of ϕ. This implies that ϕ is likely the dominant factor in emulsion rupture, rather than droplet size. More detailed theoretical support will be provided in section 3.3.1, which elaborates on the rupture details of Pickering emulsions.

3.2.4. The contact model of Pickering emulsion

To gain a better knowledge of the rheological properties of Pickering emulsions, it is essential to fully comprehend their stress–strain relationship. Therefore, it is necessary to establish a contact model for the stress–strain curves of Pickering emulsions.

Considering that the deformation of emulsions is mainly influenced by the size of the droplets, nominal stress–strain curves of emulsions with different droplet sizes on hydrophilic and hydrophobic surfaces are collected (Fig. S6(a)). Additionally, the mechanical responses for three sizes of oil droplets on the hydrophilic surface are also included in the figure. To derive the master stress–strain curve of the emulsion, it's essential to align mechanical curves under various conditions as closely as possible through normalization. The stress values at intermediate strain levels are then selected for normalization according to the traits of the curves. As depicted in Fig. S6(b-d), by normalizing the stress with the values at the strain of 0.3, all the curves are found to be converging. Polynomial functions with varying powers are adopted to fit the curve based on the characteristics of the normalized curves. The fit is evaluated by calculating the Sum of Squares for Error (SSE), as shown in Fig. S7. It's observed that the SSE value becomes greatly reduced once the polynomial degree reaches the 3rd order. A 3rd order polynomial is thus chosen to fit the normalized curves, as demonstrated in Fig. 6. The fitted equation is as follows:

$$\frac{\sigma}{\sigma_{0.3}} = 48.2\varepsilon^3 - 18.2\varepsilon^2 + 4.1\varepsilon \quad (2)$$

where $\frac{\sigma}{\sigma_{0.3}}$ is the normalized stress by the corresponding stress with a strain of 0.3. Hence, as long as the required stress at a strain of 0.3 ($\sigma_{0.3}$) for a given emulsion, which can be considered as a material parameter is obtained, the stress–strain profile of the emulsion in the deformation stage can be calculated with normalized stress ($\frac{\sigma}{\sigma_{0.3}}$). Specifically, $\sigma_{0.3}$ can be regarded as the equivalent modulus (E') of the emulsion. E' for the emulsions with different ϕ and droplet sizes are illustrated in Fig. S8. It's found that the increase in droplet size leads to a reduction in the stress required for the Pickering emulsion to achieve the same deformation. The precise relationship between the $\sigma_{0.3}$ and droplet size can be obtained by fitting statistical data of emulsions with varying droplet sizes in future studies. In addition, when working with small-sized Pickering emulsions, it's important to make subtle adjustments to account for the influence of the JJNP shells on the stress values.

As the wettability of solid surfaces is altered, Pickering emulsions may rupture after deformation, as illustrated in Fig. 4. A complete contact model can be further derived and the stress of any Pickering emulsion in contact with solid surfaces can be expressed as a product of three contributions:

$$\sigma(w, \phi, \varepsilon, r) = E'(r) \bullet f(\varepsilon) \bullet f(w, \phi) \quad (3)$$

Where $E'(r)$ represents the equivalent modulus (material property) which is dependent on the size of emulsions (r), while $f(\varepsilon)$ is the function that describes the contribution of the strain (deformation), with its expression defined in eq. (2). The product $E'(r) \bullet f(\varepsilon)$ thus characterizes the deformation characteristics of Pickering emulsion. Additionally, $f(w, \phi)$ depends on the wettability of the solid surface (w) and JNP surface coverage (ϕ), which together determine whether the emulsion will rupture during deformation. The critical deformation (ε_c) at which

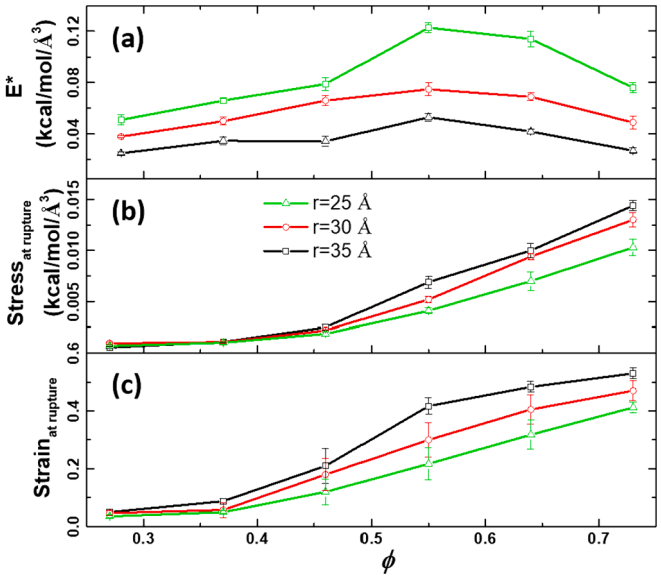

Fig.5. Effect of droplet size in the nanoscale compression of emulsion. (a) The reduced elastic modulus (E^*), (b) stress at rupture, and (c) strain at rupture as a function of ϕ for different droplet sizes.

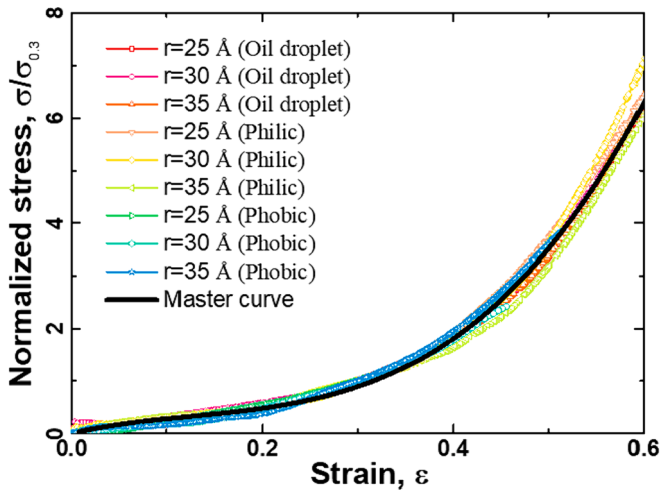

Fig.6. The normalized stress–strain curves for different compression cases and the master curve. Oil droplet, Philic, and Phobic in brackets represent the compression of an oil droplet on the hydrophilic surface, the compression of Pickering emulsion on the hydrophilic surface, and the compression of Pickering emulsion on the hydrophobic surface, respectively.

rupture occurs is thus controlled by these two variables.

3.3. Rupture mechanism of the Pickering emulsion

Due to the difficulty of characterization, the rupture details of Pickering emulsion on solid surfaces have not been investigated by previous experimental studies. Here, the rupture mechanism of the Pickering emulsion on the hydrophobic surface is investigated by quantifying the shielding effect of the JNP shell and clarifying the differences in shell structures under various JNP surface coverages.

3.3.1. Shielding effect of JNP shell in contact area with the solid surface

To quantify the shielding effect of the JNP shell, the number percentage of hydrophilic beads of JNPs (R_{JNP}) in contact area with the solid surface is calculated:

$$R_{JNP} = N_{JNP}/(N_{JNP} + N_{oil}) \quad (3)$$

According to the schematic diagram in Fig. 7(a), emulsion molecules located within a distance of 12 Å from the solid surface are identified and extracted as the contact area with the solid surface. In the eq. (3), N_{JNP} represents the number of hydrophilic beads of JNPs in the contact area while N_{oil} is the number of oil molecules. The relationship between R_{JNP} and the strain in the compression of Pickering emulsion (with different ϕ while same size) is illustrated in Fig. 7(b). The rupture moments are represented by solid markers, and the corresponding R_{JNP} at such moment is taken as the critical R_{JNP}. For the cases, with the increase of the strain, the R_{JNP} in each group decreases at a different rate and drops rapidly after the rupture of Pickering emulsions. In other words, the increasing stress leads to an intensification of the emulsion deformation in the compression. The increased deformation continuously reduces the density of JNPs on the contact area and thus weakens the shielding effect of the JNP shell. Once the shielding effect is reduced to the critical value, the Pickering emulsion ruptures.

Furthermore, ϕ greatly affects the relationship between R_{JNP} and strain (Fig. 7(b)). At the initial stage of compression (i.e., the ultra-small strain period), the R_{JNP} of the emulsion in the case with small ϕ decreases dramatically, while that of the emulsion with large ϕ maintains at a high level. It can be speculated that the JNP shell of the emulsion with large ϕ is more structurally ordered and stable than that of emulsions with small ϕ. It's worth noting that although the strain at rupture of emulsion increases with ϕ, the critical R_{JNP} can only rise to around 0.66 with increasing ϕ. This implies that when ϕ reaches a certain value, only emulsions with JNP shells on the interface with a density greater than 0.66 can be effectively shielded, and thus maintain mechanical stability. Such a view is further confirmed by emulsions with different sizes (as shown in Fig. 7(c)). The pattern of critical R_{JNP} change with ϕ is almost the same for different sizes of emulsions: the critical R_{JNP} increases with ϕ and keeps stable at a certain level (0.66–0.69). Thus, the critical R_{JNP}, which determines the rupture of the emulsion, is mainly affected by ϕ rather than droplet size. In addition, taking the emulsions with ϕ of 0.73 as the representative, the influence of the droplet size on the variation of R_{JNP} with strain is recorded in Fig. S9. It has been observed that the weakening rate of the shielding effect of the JNP shell during compression is influenced by the droplet size of the emulsion, with larger droplet sizes resulting in a slower decrease of R_{JNP} with strain. In other words, the rate of R_{JNP} decrease is inversely proportional to the droplet size of the emulsion.

3.3.2. Critical JNP surface coverage (ϕ_c)

It has been noticed that the emulsions of ϕ greater than 0.55 hold constant critical R_{JNP} and withstand high rupture stress. This is markedly different from the rupture properties of other emulsions with smaller ϕ. Such difference is most likely attributed to the unique structure of the JNP shell. The average shortest distance (D_n) between JNPs is employed to quantify the JNP stacking structure of Pickering emulsions with different ϕ after 50-ns equilibration in water.

$$D_n = \frac{\sum_{i=1}^{6}\sqrt{(x_i - x_n)^2 + (y_i - y_n)^2 + (z_i - z_n)^2}}{6} \quad (4)$$

where n represents the identifier of JNPs on the emulsion while i is the serial number of the nearest JNPs. Thus, D_n computes the mean of the distances between each JNP in the emulsion and its 6 nearest JNPs. The frequency distributions of D_n for emulsions with different ϕ are plotted in Fig. 8(a). Interestingly, the distribution of D_n is significantly variable for emulsions with ϕ less than 0.55, whereas it is more narrowed for emulsions with larger ϕ. This indicates that if ϕ is small, defects may exist in the JNP shell structure, resulting in the easy rupture of the emulsion under stress (Fig. 4(b)). When ϕ reaches 0.55, JNPs form a highly ordered stacking structure as the effective protection shell. This observation is consistent with many experiments that have observed square or hexagonal-ordered structures of NPs shells on the droplet surface, which is inspiring for optimizing nanoparticle surface coverage in applications [49,50].

In addition, the structural change (represented by D_n variation) of the initially ordered JNP shells during compression is also depicted in Fig. 8(b). When the emulsion with ϕ of 0.55 is compressed (red curve in Fig. 8(b)), the average distance between adjacent JNPs increases while D_n can still maintain relatively narrowed. At the rupture moment, abnormally large gaps appear between JNPs, which are identified by the

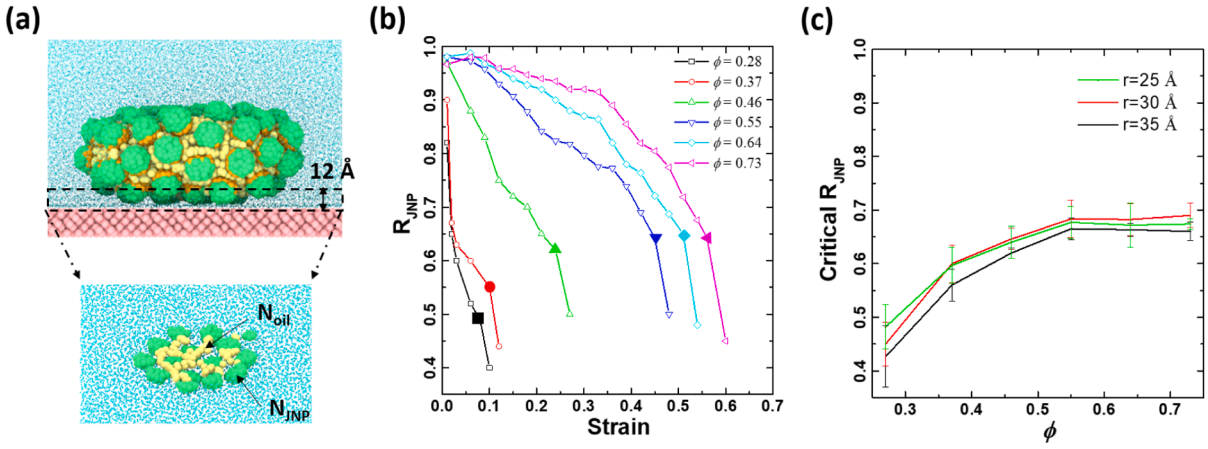

Fig.7. (a) The schematic diagram of the calculation region. The bottom graph presents the top view of the region marked in the black dotted box in the top snapshot. (b) The R_{JNP} of emulsions with respect to the strain of the emulsions in compression. Solid markers on the curves are the rupture moments. (c) Change of critical R_{JNP} with ϕ for emulsions with different droplet sizes.

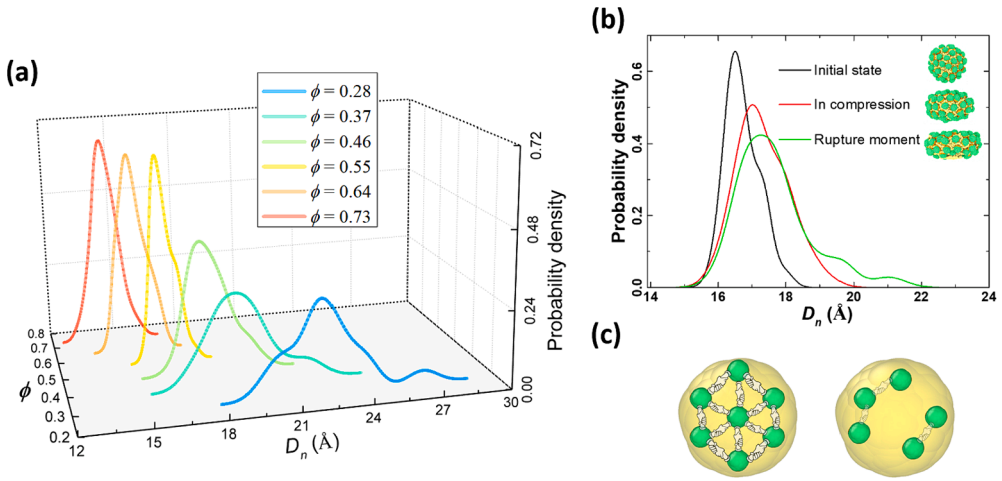

Fig.8. The structure of the JNP shell. (a) The frequency distribution of D_n with respect to distinct ϕ. (b) The frequency distribution of D_n for emulsions with ϕ of 0.55 at three moments in the compression. (c) The schematic diagram of the ordered quasi-solid structure on the left and the loose structure on the right.

wavy tail on the rightmost of the D_n distribution curve (green curve in Fig. 8(b)). It's understandable that the oil molecules are able to escape from the core to the hydrophobic surface through such vacancies. Hence, it can be concluded that once ϕ reaches the critical value, the JNPs of the emulsion form an ordered and tightly packed structure (displayed on the left side of Fig. 8(c)). Such a structure is able to effectively act as a protection shell for the oil core. During the initial stage of compression, the spacing between JNPs gradually increases while the overall structure remains relatively stable. As the emulsion continues to deform, part of the shell structure is gradually destroyed and transformed into a loose structure (as depicted on the right side of Fig. 8(c)), which then causes the oil core to leak from vacancies due to the attraction of the surface. This eventually leads to the collapse of the emulsion under pressure.

4. Conclusions

The deformation and rupture characteristics of Janus nanoparticle (JNP) stabilized Pickering emulsions on solid surfaces are revealed with the nanoscale compression test using molecular dynamics (MD) simulations. It was shown that the droplet size has a more pronounced effect on the mechanical properties of Pickering emulsions during the deformation stage, compared to the surface coverage (ϕ). The universal behavior of the emulsion in compression can be predicted with a contact model. Moreover, the compressed Pickering emulsions rupture on the hydrophobic surface due to the strong attraction forces. ϕ is the key factor affecting the rupture. Once ϕ reaches a critical value, the JNP shell can form a highly ordered structure, which effectively protects the oil core and remarkably enhances the stability of emulsion in contact with the solid surface. These findings not only provide a new approach for predicting the mechanical deformation, but also reveal the governing parameter for rupture of Pickering emulsions. This will ultimately provide guidelines for the design, screening, modification, and application of Pickering emulsions.

CRediT authorship contribution statement

Yuanhao Chang: Conceptualization, Writing – original draft. **Senbo Xiao:** Methodology, Software. **Rui Ma:** Software. **Zhiliang Zhang:** Supervision, Writing – review & editing. **Fanhua Zeng:** Supervision, Writing – review & editing. **Jianying He:** Writing – review & editing.

Declaration of competing interest

The authors declare that they have no known competing financial interests or personal relationships that could have appeared to influence the work reported in this paper.

Data availability

Data will be made available on request.

Acknowledgements

This work was financially supported by the Research Council of Norway (Grant No. 234626). The supercomputer CPU hours were provided by the Norwegian Metacenter for Computational Science (Grant No. NN9110K and NN9391K).

Appendix A. Supplementary data

Supplementary data to this article can be found online at https://doi.org/10.1016/j.cej.2024.150355.

References

[1] P.S. CXCVI, Emulsions, J. Chem. Soc. Trans 91 (1907) 2001–2021.
[2] W. Ramsden, Separation of solids in the surface-layers of solutions and 'suspensions'(observations on surface-membranes, bubbles, emulsions, and mechanical coagulation).—Preliminary account, Proc. Royal Soc. Lond. 72 (477-486) (1904) 156–164.
[3] B.P. Binks, Particles as surfactants—similarities and differences, Curr. Opin. Colloid Interface Sci. 7 (1–2) (2002) 21–41.
[4] N. Yan, M.R. Gray, J.H. Masliyah, On water-in-oil emulsions stabilized by fine solids, Colloids Surf. A Physicochem. Eng. Asp. 193 (1–3) (2001) 97–107.
[5] T.S. Horozov, et al., Order– disorder transition in monolayers of modified monodisperse silica particles at the octane– water interface, Langmuir 19 (7) (2003) 2822–2829.
[6] X. Lu, M. Wang, Shape and surface property effects on displacement enhancement by nanoparticles, Int. J. Mech. Sci. 255 (2023) 108471.
[7] J. Choi, et al., Hydrophobically modified silica nanolaces-armored water-in-oil pickering emulsions with enhanced interfacial attachment energy, J. Colloid Interface Sci. 641 (2023) 376–385.
[8] H. Yang, et al., Compartmentalization of incompatible reagents within Pickering emulsion droplets for one-pot cascade reactions, J. Am. Chem. Soc. 137 (3) (2015) 1362–1371.
[9] J. Huang, et al., pH-responsive gas–water–solid interface for multiphase catalysis, J. Am. Chem. Soc. 137 (47) (2015) 15015–15025.
[10] J. Xu, et al., Synthesis of Au and Pt hollow capsules with single holes via pickering emulsion strategy, J. Phys. Chem. C 119 (50) (2015) 28055–28060.
[11] J. Xu, et al., Hierarchical CuO colloidosomes and their structure enhanced photothermal catalytic activity, J. Phys. Chem. C 120 (23) (2016) 12666–12672.
[12] M.A. Hussein, A.A. Mohammed, M.A. Atiya, Application of emulsion and Pickering emulsion liquid membrane technique for wastewater treatment: an overview, Environ. Sci. Pollut. Res. 26 (2019) 36184–36204.
[13] H. Li, et al., Pickering emulsion enhanced interfacial catalysis under Taylor flow in a microchannel reactor, Chem. Eng. J. 466 (2023) 143258.

[14] B.M. Trinh, M. Smith, T.H. Mekonnen, A nanomaterial-stabilized starch-beeswax Pickering emulsion coating to extend produce shelf-life, Chem. Eng. J. 431 (2022) 133905.
[15] D. Voorn, W. Ming, A. Van Herk, Polymer– clay nanocomposite latex particles by inverse pickering emulsion polymerization stabilized with hydrophobic montmorillonite platelets, Macromolecules 39 (6) (2006) 2137–2143.
[16] T. Zhang, et al. 2010. Nanoparticle-stabilized emulsions for applications in enhanced oil recovery. in SPE improved oil recovery symposium. OnePetro.
[17] H. Li, et al., Pickering gel emulsion of lipiodol stabilized by hairy nanogels for intra-artery embolization antitumor therapy, Chem. Eng. J. 418 (2021) 129534.
[18] A.S. Meimanova, et al., Spatio-temporally resolved dynamical transitions in flow of Pickering emulsions through porous media, Chem. Eng. J. (2023) 147699.
[19] S.-Y. Tan, et al., Nano-mechanical properties of clay-armoured emulsion droplets, Soft Matter 8 (11) (2012) 3112–3121.
[20] D. Hatchell, W. Song, H. Daigle, Effect of interparticle forces on the stability and droplet diameter of Pickering emulsions stabilized by PEG-coated silica nanoparticles, J. Colloid Interface Sci. 626 (2022) 824–835.
[21] C. Griffith, H. Daigle, On the shear stability of water-in-water Pickering emulsions stabilized with silica nanoparticles, J. Colloid Interface Sci. 532 (2018) 83–91.
[22] W. Li, et al., Recent advances on pickering emulsions stabilized by diverse edible particles: Stability mechanism and applications, Front. Nutrit. (2022) 738.
[23] L.E. Low, et al., Recent advances of characterization techniques for the formation, physical properties and stability of Pickering emulsion, Adv. Colloid Interface Sci. 277 (2020) 102117.
[24] Y. Chevalier, M.-A. Bolzinger, Emulsions stabilized with solid nanoparticles: Pickering emulsions, Colloids Surf. A Physicochem. Eng. Asp. 439 (2013) 23–34.
[25] D.G. Ortiz, et al., Current trends in Pickering emulsions: Particle morphology and applications, Engineering 6 (4) (2020) 468–482.
[26] I. Klojdová, C. Stathopoulos, The potential application of Pickering multiple emulsions in food, Foods 11 (11) (2022) 1558.
[27] M. AfzaliTabar, et al., Facile and economical preparation method of nanoporous graphene/silica nanohybrid and evaluation of its Pickering emulsion properties for Chemical Enhanced oil Recovery (C-EOR), Fuel 206 (2017) 453–466.
[28] K.-K. Liu, Deformation behaviour of soft particles: A review, J. Phys. D Appl. Phys. 39 (11) (2006) R189.
[29] J.K. Ferri, et al., Separating membrane and surface tension contributions in Pickering droplet deformation, Soft Matter 4 (11) (2008) 2259–2266.
[30] Z. Wang, et al., Molecular dynamics-based simulation on chemical flooding produced emulsion formation and stabilization: a critical review, Arab. J. Sci. Eng. 45 (2020) 7161–7173.
[31] T. Lu, et al., Stability and enhanced oil recovery performance of CO2 in water emulsion: Experimental and molecular dynamic simulation study, Chem. Eng. J. 464 (2023) 142636.
[32] H. Fan, A. Striolo, Mechanistic study of droplets coalescence in Pickering emulsions, Soft Matter 8 (37) (2012) 9533–9538.
[33] H. Jia, et al., Potential application of novel amphiphilic Janus-SiO_2 nanoparticles stabilized O/W/O emulsion for enhanced oil recovery, Colloids Surf. A Physicochem. Eng. Asp. 622 (2021) 126658.
[34] L. Martínez, et al., PACKMOL: A package for building initial configurations for molecular dynamics simulations, J. Comput. Chem. 30 (13) (2009) 2157–2164.
[35] M.G. Martin, J.I. Siepmann, Transferable potentials for phase equilibria. 1. United-atom description of n-alkanes, J. Phys. Chem. B 102 (14) (1998) 2569–2577.
[36] V. Molinero, E.B. Moore, Water modeled as an intermediate element between carbon and silicon, J. Phys. Chem. B 113 (13) (2009) 4008–4016.
[37] R. Ma, et al., An interfacial gas-enrichment strategy for mitigating hydrate adhesion and blockage, Chem. Eng. J. 453 (2023) 139918.
[38] Y. Chang, et al., Atomistic insight into oil displacement on rough surface by Janus nanoparticles, Energy 245 (2022) 123264.
[39] Y. Chang, et al., Nanomechanical characteristics of trapped oil droplets with nanoparticles: A molecular dynamics simulation, J. Pet. Sci. Eng. 203 (2021) 108649.
[40] S. Plimpton, Fast parallel algorithms for short-range molecular dynamics, J. Comput. Phys. 117 (1) (1995) 1–19.
[41] A. Stukowski, Visualization and analysis of atomistic simulation data with OVITO–the open visualization tool, Model. Simul. Mater. Sci. Eng. 18 (1) (2009) 015012.
[42] S. Nosé, A unified formulation of the constant temperature molecular dynamics methods, J. Chem. Phys. 81 (1) (1984) 511–519.
[43] W.G. Hoover, Canonical dynamics: Equilibrium phase-space distributions, Phys. Rev. A 31 (3) (1985) 1695.
[44] X.C. Luu, J. Yu, A. Striolo, Nanoparticles adsorbed at the water/oil interface: coverage and composition effects on structure and diffusion, Langmuir 29 (24) (2013) 7221–7228.
[45] A. Haji-Akbari, P.G. Debenedetti, Direct calculation of ice homogeneous nucleation rate for a molecular model of water, Proc. Natl. Acad. Sci. 112 (34) (2015) 10582–10588.
[46] M. Saifullah, A. Ahsan, M.R.I. Shishir, Production, stability and application of micro-and nanoemulsion in food production and the food processing industry, in: Emulsions, Elsevier, 2016, pp. 405–442.
[47] S. Mettu, et al., Ultrasonically synthesized organic liquid-filled chitosan microcapsules: part 2: Characterization using AFM (atomic force microscopy) and combined AFM–confocal laser scanning fluorescence microscopy, Soft Matter 14 (16) (2018) 3192–3201.
[48] A. Fischer-Cripps, The Hertzian contact surface, J. Mater. Sci. 34 (1) (1999) 129–137.
[49] J. Xu, et al., Investigation of the contact angle and packing density of silica nanoparticles at a pickering emulsion interface fixed by UV polymerization, Langmuir 38 (14) (2022) 4234–4242.
[50] D. Ershov, et al., Capillarity-induced ordering of spherical colloids on an interface with anisotropic curvature, Proc. Natl. Acad. Sci. 110 (23) (2013) 9220–9224.